Temperature-dependence of the static contact angle: A transition state theory approach

Benoît Duchemin, Guillaume Cazaux, Moussa Gomina, Joël Bréard

Temperature-dependence of the static contact angle: a transition state theory approach (preprint)

Benoît Duchemin[a,*], *Guillaume Cazaux*[a,1], *Moussa Gomina*[b], *Joël Bréard*[c]
[a] Normandie Université, UNIHAVRE, CNRS, LOMC, 76600 Le Havre, France
[b] Normandie Université, ENSICAEN, CNRS, CRISMAT, 14000 Caen, France
[c] Normandie Université, UNICAEN, UNIROUEN, ABTE, 14000 Caen, France

***Corresponding author.**
E-mail address: benoit.duchemin@univ-lehavre.fr
Tel: +33.2.35.21.71.54
[1] Current address : Asco Industries, Zaventem, Belgium

Abstract
The temperature dependence of the static contact angle could *a priori* be predicted by using surface tension partitioning. An original model based on the transition state theory is also introduced. This model considers thermocapillary fluctuations on the droplet surface near the triple line and the self-affine pinning of this triple line against a solid substrate modelled with a pseudo-periodic distribution of adsorption sites. The temperature dependence of the static contact angle was studied for a representative range of liquids with different polarities and on a wide array of solid substrates for temperatures ranging from 25 to 240°C. Atomic force microscopy (AFM) was also used to quantify the surface roughness of the solid substrates. Whereas the surface tension partitioning failed to bring consistent results above room temperature, the transition state model proved very useful, thereby opening a way to yield predictive contact angle values with temperature variations. The introduction of a topological dimension in the equations yields a unified model that covers normal wetting (perfectly bonded liquids on smooth surfaces) but also the onset of Cassie-Baxter and Wenzel states on real surfaces. Moreover, the model encompasses the transition to complete wetting.

1. Introduction

The physics of wetting is a topic of active research with an extremely broad range of practical applications. Daily applications cover the spreading of common liquids such as detergents on domestic surfaces, fungicides on plants or cosmetics for hair and skin. In the last two decades, a great deal of research has also been devoted to the modification of solid surfaces in order to produce surfaces displaying superhydrophobicity, superoleophobicity or superhydrophilicity.[1–4] These advanced surfaces often combine a chemical treatment and a roughness modification. These combinations of tailored geometry and chemical modifications spectacularly expand the functionalities of traditional coatings. As a result, novel coatings with specific anti-fingerprint, anti-fouling, non-wetting, non-adhesive or self-cleaning properties have become an industrial reality. All of the above-mentioned surfaces are exposed to a wide temperature range in working conditions. It is thus of importance to understand the impact of temperature variations on surface tensions and contact angles. Such thermal variations are ubiquitous: the spreading of water droplets on a boat hull or that of an oil droplet in a frying pan are common examples.

The surface tension and surface free energy of liquids and solids are not constant with temperature. Both of them are known to vary linearly with the temperature of the system.[5–10] The first theoretical studies devoted to the variation of surface tension of liquids as a function of temperature date back to the end of the 19th century and are attributed to Loránd Eötvös.[5,11] Eötvös understood the variation of surface tension with temperature in the light of van der Waals' equation of state and of the principle of corresponding states. He expressed this dependence in a surprisingly simple form:

$$\gamma_l \, . \, V_m^{2/3} = \kappa.(T_0 - T) \qquad (1)$$

Where γ_l is the liquid surface tension, V_m is the molecular volume, κ is a constant, T_0 is a temperature close to the critical temperature of the liquid and T the temperature at which the experiment is performed.[5,12–14] While this mathematical formulation is working strikingly well with the usual non-polar liquids, and to a lesser extent with polar liquids, the Eötvös κ constant is specific to each liquid.[5,8,12,13] Eötvös' law has been reinterpreted on theoretical grounds and proved a valid heuristic model when the vapor density is negligible compared with the liquid density.[12–14] A particular interpretation of this equation relies on Gibbs' free energy formulation ($\Delta G = \Delta H - T.\Delta S$). The constant κ is then understood as the entropy change when liquid molecules migrate from the core of the liquid to the surface.[12,13,15] These considerations help explaining why hydrogen-bonded "structured" liquids such as water or alcohols usually have a lower entropy change than non-polar liquids.[5,11–13] Early corrections to Eötvös' law were also proposed by Katayama, Ramsay and Shields to account for surface tension nonlinearities near T_c, but these

corrections are of little use in narrow working ranges above the liquid melting temperature and far from its critical temperature.[8,11,13] Aside the Eötvös' model, other theoretical models also exist. For instance, a power-law model (sometimes named the Katayama-Guggenheim model) was also introduced by Ferguson and later backed up by Guggenheim's demonstration using the principle of corresponding states.[8,16,17] However, this model was restricted to non-polar liquids. The Flory, Orwoll and Vrijj equation of state theory can also be used to predict surface tension from PVT data.[18–20] Nonetheless, this last approach requires specific equipment whereas Eötvös' law can be confirmed by surface tension measurements using the widely available pendant drop method.

Whereas it is usually straightforward to explain the thermal variations of the surface tension, the variations of the contact angles with temperature are not as easy to explain. There exist several works in the literature dedicated to the variation of the static contact angle θ_s as a function of the temperature. As a general rule, the contact angle is found to decrease with an increasing temperature; however, some rare systems show the opposite behavior.[21] Furthermore, the literature shows disagreements as to the type of equation linking θ_s and temperature. For instance, De Ruijter *et al.* measured a linear dependency of the contact angle θ_s on the temperature for the squalane/PET system.[22] Petke and Ray also found a linear relationship between temperature and contact angle for a range of liquids on polymer surfaces.[23] Other authors found a different result with a linear dependency of $\cos\theta_s$ on temperature.[24,25] Another more general view based on Gibbs adsorption isotherm and Polyani adsorption theory is that of a power-law dependency of $\cos\theta_s$ on T; this view has the advantage of including the linear dependency of some other systems in a relatively narrower temperature range.[26,27] Eventually, another work reports complex θ_s variations of *n*-decane on PTFE; the variations show singularities attributed to the various viscoelastic relaxations of PTFE in the studied temperature range.[28] Therefore, there seems to be no general model to describe these variations. To the best of our knowledge, surface tension partitioning has never been used to assess the temperature dependence of the contact angle, despite the popularity of this method.[9,29–32] Interestingly, the *dynamic* contact angle θ_d can be well described using Eyring's reaction rate theory at small capillary numbers.[22,24,33–37] In this theory, the rate of a liquid molecule jumping in or out of an active site located at the solid surface near the triple line determines the triple line speed. In this theory, the temperature is an explicit variable.

The present work is therefore purported to the study of the liquid surface tension and to the temperature-dependence of the static contact angle. The study was carried out using a simple goniometer enabling the determination of the liquid surface tensions and contact angles over a wide temperature range. Six liquids with various polarities were tested over temperatures comprised between 25°C and 240°C. These liquids were tested against a set of surfaces with different surface energies, including PTFE as a non-polar surface, glass, ceramics and metallic materials. The effect of temperature was assessed in the light of the surface tension partitioning method, and in the light of a novel alternative model based on the transition state theory. In the latter, a novel view was proposed that correlates the amplitude of surface waves and the self-similar distortions of the triple line near real surfaces modeled with a pseudo-periodic distribution of adsorption sites.

2. Descriptive models:

2.1. *Calculation of the dispersive component of the liquids at various temperatures*

It is possible to give a predictive interpretation of the surface tension by looking at the contribution of the non-covalent forces responsible for the stability of condensed matter. These forces include the van der Waals (vdW) forces (Keesom, Debye and London forces), hydrogen bonding and acid-base forces in general, Coulombic interactions and metallic bonds. According to van Oss, Good and Chaudury, the surface tension can be expressed as:

$$\gamma = \gamma^{LW} + \gamma^{AB} \qquad (2)$$

The three electrodynamic vdW forces are additively grouped together in the long-range Lifshitz-van der Waals surface tension component γ^{LW}. The other "polar" forces induced by the strong asymmetry of electrostatic components are accounted for in the Lewis acid-base γ^{AB} component.[9,38] γ^{AB} results from the combination of two components: an electron donor γ^- component and an electron acceptor γ^+ component. Of considerable practical importance, hydrogen-bonding interactions are considered as a subset of the more general Lewis acid-base interactions. This partition constitutes a different view to that of Owens and Wendt or Fowkes, who considered that the surface tension was the sum of a γ^d surface tension covering the dispersion forces (London) and a γ^h surface tension grouping together the other electrodynamic dipole-dipole and hydrogen bonding interactions.[32,39] All surface tension partitioning models have been used in combination with Berthelot's geometric means principle to evaluate the interactions between two immiscible phases across an interface.[39,40] According to Van Oss *et al.*, the interfacial free energy γ_{sl} between a liquid (subscript *l*) and a solid (subscript *s*) can be written as:

$$\gamma_{sl} = \gamma_s + \gamma_l - 2.(\gamma_s^{LW}.\gamma_l^{LW})^{½} \qquad (3)$$

provided that at least one of the components (liquid or solid) is apolar.[9,30,41] This hypothesis is satisfied for solids such as PTFE or liquids such as methylene iodide, meaning that

their surface free energy γ is approximated by γ^{LW}. Surface tension partitioning is also often used in conjunction with the Young-Dupré equation in order to predict the contact angle formed by a liquid droplet on a surface.[30,39] Neglecting the spreading pressure, the static contact angle can be introduced in the form of:

$$\gamma_l(1 + \cos\theta_s) = 2.(\gamma_s^{LW}.\gamma_l^{LW})^{½} \quad (4)$$

Where θ_s is the static contact angle.[9,32,39] The spreading pressure can be neglected in the case of low surface energy solids such as polymers or oxides with a contaminated surface, *i.e.* oxides that have been left to equilibrate with the atmosphere after cleaning, polishing of cleavage.[42] Once surface tension partitions are determined for several liquids (at several temperatures, in the present case), it should become possible to estimate the solid surface tension partition of any set of solid substrates.

2.2. Alternative model: a transition state approach

A description of the static contact angle as a function of temperature is introduced in this paragraph. This view is solely based on physical considerations around the specific case of partial wetting of small monomolecular liquids; the cases of liquid macromolecules or colloids need to integrate obvious corrections such as collective displacement, interfacial repulsion or adsorption and specific Brownian motion. Thermal noise needs to be introduced first: it is well-known that the surface of liquids bears a certain roughness due to the existence of thermally excited capillary waves that introduce surface fluctuations.[43–46] The roughness of these surface waves is proportional to:

$$\xi = \sqrt{\frac{k_B T}{\gamma_l}} \quad (5)$$

Where k_B is the Boltzmann constant, T is the temperature and γ_l is the liquid surface tension. Consequently, ξ is the characteristic length (also known as the thermal length) of the problem and its theoretical value is in the order of 2-3 Å.[43,47,48] The measured root-mean-square amplitude of surface waves has been measured at ~5-7 Å for liquids such as alkanes or ethanol.[44,45] In recent works, it has been shown that the thermal fluctuations at the liquid-gas interface expand all the way to the triple line.[48]

The triple line has so far been described as a discontinuity anchored (or *pinned*) microscopically on a chemically heterogeneous surface; the bound states of liquid molecules are due to the presence of periodically arranged "weak heterogeneities" on the surface of the substrate.[7,49–51] Triple line pinning has a typical length scale around 1 nm, which is in the same order of magnitude as ξ.[7,49,50] However, the coupling between thermal fluctuations and liquid binding at the solid surface has never been used to provide useful scaling arguments related to the triple line description, to the best of our knowledge.

The demonstration is based on the application of the theory of absolute reaction rates, in a spirit similar to that developed in the pioneering work of Blake and Haynes (1969).[34,52,52,53] If one imagines that a liquid molecule at the triple line jumps forward and is adsorbed, the rate constant can be expressed as :

$$k_{ads} = \tau \frac{F_{ads}^{\ddagger}}{F_{norm}} \frac{k_B T}{h} e^{\frac{-E_{ads}}{k_B T}} \quad (6)$$

Where τ is the transmission coefficient, also known as the steric factor; it allows for all the collisions not be effective when the energy requirements are satisfied. $F_{ads}^{\ddagger}$ is the partition function for the activated site and F_{norm} is the partition function for the normal state.[54] Naturally, h is the Planck constant. The same formula can be written for desorption, when an adsorbed liquid molecule moves backwards from the gas phase to the liquid one:

$$k_{des} = \tau \frac{F_{des}^{\ddagger}}{F_{norm}} \frac{k_B T}{h} e^{\frac{-E_{des}}{k_B T}} \quad (7)$$

The transmission coefficient remains the same due to symmetry considerations. As proposed by Blake, the net rate of exchange is zero at equilibrium, thus:

$$k_{des} = k_{ads} \quad (8)$$

Therefore:

$$\frac{F_{ads}^{\ddagger}}{F_{des}^{\ddagger}} = e^{\frac{-(E_{ads}-E_{des})}{k_B T}} \quad (9)$$

This result was originally proposed by Blake and Haynes.[34] The term E_{ads}- E_{des} will simply be called activation energy $E^{\ddagger}$ in the rest of the article. This energy is required to maintain the presence of a liquid front near a statistically defined triple line at the equilibrium temperature, balancing thermocapillary effects with fast adsorption-desorption phenomena. The main hypothesis of this work is that the triple line is stochastically jumping forward and backward with an amplitude equal to that of thermocapillary waves, *i.e.* ξ. This energy can thus be expressed as:

$$E^{\ddagger} = -S.\xi^2 \quad (10)$$

Where S is the spreading parameter, corresponding to the free energy difference between a dry and a wet solid:[7,55]

$$S = \gamma_{sv} - (\gamma_{sl} + \gamma_l) \quad (11)$$

It is known that $S > 0$ corresponds to the total wetting case and $S < 0$ corresponds to the partial wetting case. Using the law of Young-Dupré, it is possible to express S as a function of Young's ideal contact angle θ_Y:[7,49]

$$S = \gamma_l(\cos\theta_Y - 1) \quad (12)$$

Because the measurements were made after the contact angles were stabilized, it is in the present work considered

that the static contact angle θ equals Young's contact angle θ_Y. This brings a macroscopic parameter that is measurable (θ) in an equation otherwise built on microscopic considerations:

$$\frac{F^{\ddagger}_{ads}}{F^{\ddagger}_{des}} = e^{\frac{\gamma_l(\cos\theta-1).\xi^2}{k_B T}} = e^{\cos\theta-1} \qquad (13)$$

Now, in the equilibrium state, one can consider that the ratio of partition functions is the ratio of a capillary wave amplitude divided by a cutoff length $< d >$. This characteristic distance ($< d >$) can be understood as the lateral correlation length between adsorption sites (or finite potential wells) placed pseudo-periodically on the surface. This concept was developed and successfully used by others in the so-called *weak pinning* framework in order to explain contact angle hysteresis.[49,51] Therefore :

$$\frac{F^{\ddagger}_{ads}}{F^{\ddagger}_{des}} = \left(\frac{\xi}{\langle d\rangle}\right)^f \qquad (14)$$

Where f is the fractal dimension of the problem: $f = 1$ for a triple line jumping straight from well to well, $1 \leq f < 2$ for a "normal" triple line thermally fluctuating around the mean path and in contact with the surface, and $2 \leq f < 3$ for a planar triple line, *i.e.* a Cassie-Baxter state with entrapped gas between the solid surface and the liquid (Figure 1). On the opposite, if "hemiwicking" takes place (Wenzel state), $f < 1$ since the liquid is channeled through the surface grooves ahead of the triple line, thereby decreasing the fraction of triple line in contact with the solid (Figure 1).

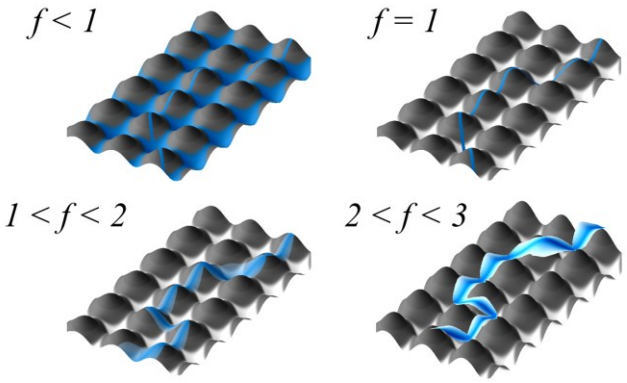

Figure 1. Putative construction of the thermally activated triple line (blue line) against a model surface with periodically arranged adsorption sites for different f values when $\xi < \langle d\rangle$. In the Wenzel state ($f < 1$), a continuous liquid phase is found between the adsorption sites, thereby shortening the effective triple line path. In the "normal" cases where the triple line is found on the solid substrate, it either travels though the centers of the adsorption sites along the shortest path ($f = 1$) or it more likely fluctuates around this mean path ($1 < f < 2$). In the Cassie-Baxter state ($2 < f < 3$), the triple line is pinned against adsorption sites but gas is also entrapped between the liquid and the substrate (on the picture, the stochastic line appears to "jump" above the surface).

In this equation, the parameters f and $< d >$ need to be determined for each {solid ; liquid} pair since each liquid will uniquely "probe" a given solid. This is due to the specificities of their chemical interplay (Van der Waals forces, hydrogen bonds, electrostatic forces, π-interactions, etc.), steric effects and the energy landscape of the solid surface. Therefore, a very simple equation is produced that describes the variations of contact angle with temperature:

$$\left(\frac{\xi}{\langle d\rangle}\right)^f = e^{\cos\theta-1} \qquad (15)$$

Or:

$$f.ln\left(\frac{\xi}{\langle d\rangle}\right) = \cos\theta - 1 \qquad (16)$$

One notices that the transition to complete wetting ($\theta = 0$) produces the equality $\xi = < d >$, meaning that the critical wetting temperature corresponds to capillary waves with an amplitude equal to the correlation distance between adsorption sites. This temperature-dependent wetting transition is documented in the literature.[7,56–60] It is sometimes abrupt and it marks the shift from a partial (or pseudo-partial) wetting characterized by a positive contact angle to a complete wetting where the liquid spreads spontaneously on the surface. The wetting transition framework can be subdivided in three different cases: the continuous long-range critical wetting that is activated by a sign change of the Hamaker constant, a discontinuous first-order transition implying a discontinuity in the first derivative of the surface free energy and the critical wetting near the critical temperature of the liquid.[57,60,61] The wetting transition is never treated in a more general theoretical framework. In this work, the transition to complete wetting can be understood as a modification of the energy landscape to the point where the activation energy between two states disappears at a critical temperature, *i.e.* the activated state and the initial state have the same energy (Figure 2). The overall slope is always negative (as expected for an infinite spreading in the complete wetting case) and the energy landscape still bears $< d >$-periodic variations corresponding to the remaining presence of adsorption sites.

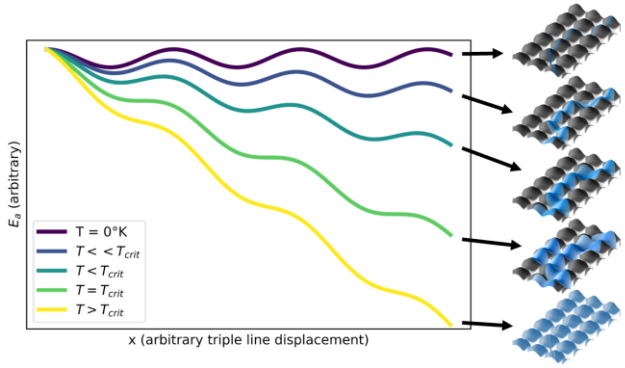

Figure 2. Conceptual view of the energy landscape involved at different temperatures. In the right column, the thermally activated triple line appears as the blue area on a model surface with periodically arranged adsorption sites (grayscale).

3. Materials and methods

3.1. Materials

The liquids used were ultrapure water (18.2 mΩ.cm), formamide (99.5%, Sigma-Aldrich, ref F9037), glycerol (99 %, Sigma-Aldrich, G5516), ethylene carbonate (99%, VWR, ref 15735-0C), methylene iodide (99.4%, VWR, ref 25633.186) and methyl benzoate (99%, VWR, ref 146024). All the liquids were used as received with no further purification.

The solids were microscope glass slides (Thermo scientific, white glass IOS 8037/1), a PTFE plate (T_m = 327°C, no additives, SS plastic industry technology, ref SDDQ-31), stainless steel (Depery Dufour, ref 304L TI15B), alumina (99.85%, Solostocks, ref Durmax-BRH), yttria-stabilized zirconia (ZrO_2 $3Y_2O_3$, J&K scientific ltd, ref 64417-98-7) and brass (Macc model engineers supplies ltd, ref 20SWG-804001). All substrates were cut to square plates with a side length of approximately 20 mm.

3.2. Methods

3.2.1. Surface preparation

All solid surfaces except the glass slides were prepared using a Struers AbraPol-10 automatic polishing machine according to the procedures recommended by the manufacturer (Metalog guide, Struers). The final polishing step yielded low roughness surfaces. This crucial step was performed using MD-Chem pads and a 40 nm colloidal silica suspension (OP-S, Struers). The surfaces were then thoroughly rinsed with distilled water. The glass slides were cleaned using distilled water, ethanol and acetone. All the samples were left for drying at room temperature for a minimum of 24 h before contact angle measurements.

3.2.2. Atomic Force Microscopy

AFM was conducted on a Brüker Innova (Bruker corp.) at 23°C and 50% RH. After polishing, the solid surfaces were cut to the appropriate dimensions and cleaned. Cleaning consisted in a 5 min immersion in a distilled water bath under ultrasonic stirring followed by a 5 min immersion in ethanol under ultrasonic stirring. The surfaces were then thoroughly rinsed with ethanol. The samples were carefully glued to the sample holders before being imaged in contact mode with a TESPA tip (290-348 kHz, 20-80 N/m, 8 nm curvature). The measurements were performed on 50x50 µm areas at a resolution of 1024*1024 pixels. A minimum of four measurements was performed for each surface. Surface roughness was then calculated using the Nanoscope Analysis V 1.40 software provided by the manufacturer after a first order flattening of each line without using any threshold. Arithmetic roughness (R_a), geometric roughness (R_g) and maximum roughness amplitude (R_{max}) were assessed and reported.

3.2.3. Surface tension and contact angle measurements

A Krüss DSA100 tensiometer equipped with a high-temperature dosing system (DO3241) and a high temperature chamber (TC21) was used. The drop shapes were acquired using a goniometer. The data were then treated using the proprietary Drop Shape Analysis 1.92.1.1 software. The surface tensions of the liquids were determined using the axisymmetric drop shape analysis method devised by Song *et al.* and implemented in the software.[62,63] The liquid densities were determined using thermal expansion parameters from the literature.[64–66] Needles 1.8 mm in diameter were used for the pendant drop method. The contact angles were measured using the tangent method. Needles 0.5 mm in diameter were used for contact angle measurements in order to keep the deformation of the drop under its own weight as small as possible (Bond number < 1). The liquids were tested between their melting point and boiling temperature, at atmospheric pressure and at 20, 40, 60, 80, 120, 140, 160, 180, 200 and 240°C.

4. Results and discussion

4.1. Atomic Force Microscopy

Topographic measurements of the six solid substrates were performed by AFM. Typical results are presented in Figure 3 and the roughness values are presented in Table 1. In general, the surfaces were rather smooth and their roughness was low, but none of these surfaces was smooth at the atomic level. However, one needs to question the dimensions of a surface geometric heterogeneity necessary to create significant effects on the macroscopic contact angle. Two major description exist: the Cassie-Baxter state and the Wenzel state.[1,67] The Cassie-Baxter state is characterized by entrapped air between the droplet and the substrate. The Cassie-Baxter state requires a long-range periodic geometric pattern on the surface; it is also favored by a high aspect ratio, a short periodicity (or short pitch) of the pattern, a low surface free energy (such as that provided by polymer surfaces) and a low hydraulic pressure of the drop against the surface.[1,4,67] In contrast, the Wenzel state hypothesizes a perfect contact between the liquid and the solid substrate. The latter state forms a continuum with the ideal case of a perfectly smooth surface in the geometrical acceptance of the "smooth" term. In this state, the liquid wets through the surface grooves and "hemiwicking" takes place.[1] In this work, the surfaces display a roughness devoid of periodicity (Figure 3). PTFE occupies a special place in this work because of its low surface free energy known to be largely apolar (or hydrophobic). Its typical roughness lies in the low roughness range usually observed in Cassie-Baxter states, usually in the 200 nm–30 µm range (Table 1).[1,4] Therefore, the possibility of existing Cassie-Baxter states on this surface cannot be completely discarded. Alumina and zirconia had the highest roughness, which makes them more likely to induce Cassie-Baxter or Wenzel states, depending on the liquids used.

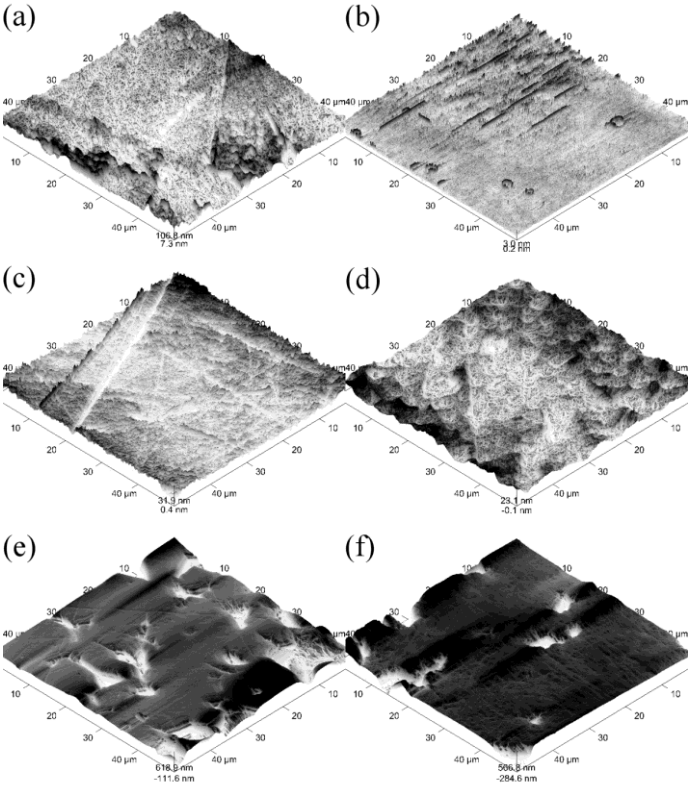

Figure 3. Topography images of (a) PTFE, (b) glass, (c) brass, (d) stainless steel, (e) alumina and (f) yttria-stabilized zirconia.

Table 1. Arithmetic, quadratic and maximum roughness as measured by AFM

Sample	R_a *(nm)*	R_q *(nm)*	R_{max} *(nm)*
PTFE	19.3 ± 2.0	26.2 ± 2.2	288.7 ± 54.5
Glass	0.8 ± 0.1	1.6 ± 0.5	93.3 ± 15.5
Brass	6.4 ± 0.7	8.3 ± 1.0	103.9 ± 20.1
Stainless steel	7.7 ± 2.3	9.7 ± 2.8	110.5 ± 67.7
Alumina	86.5 ± 29.7	140.5 ± 37.5	1505.1 ± 304.4
Yttria-stabilized zirconia	281.5 ± 164.7	460.3 ± 246.9	4427.7 ± 1480.1

4.2. Surface tensions

The surface tensions of the liquids were measured using the pendant drop method. The results are shown on Figure 4. The raw data as well as plots comparing the data against literature values are supplied as Supplementary Information. The surface tensions decrease linearly with the temperature and the overall values are generally consistent with literature data.[5,13,68,69] Therefore, the data follows Eötvös' law very well. As to the slopes, Pászli and Lászó report values between -79 and -189 $\mu J.m^{-2}.K^{-1}$. The room temperature values compare accurately against reported and commonly admitted values (Figure 4, Table 2 and SI). However, some deviations are sometimes observed at higher temperatures. For instance, methyl benzoate has a larger slope than values reported eleswhere.[68,69] Some deviations can be explained by the fact the liquids were used "off the shelves" (i.e. with no purification), and other deviations might be explained by the experimental setup. The experimental setup made use of steel needles, and the liquids were exposed to an oxidizing atmosphere or to visible light (to which methylene iodine is sensitive). The densities were chosen from literature values. Different operators and measurement techniques (Wilhelmy blade *versus* pendant drop) can also account for these minor discrepancies. Since no hypothesis is made regarding the absolute purity of the liquids used, the deviations within and against reported values do not diminish the usefulness of the data in any way: the reported measurements on such a wide temperature range are scarce. Furthermore, the literature values are sometimes ancient and would therefore require confirmations by other groups (with the exception of water).

In this work, several other points are worth noting. Three liquids were capable of forming hydrogen bonds among the six liquids considered here: water (capable of forming four hydrogen bonds), glycerol (capable of three hydrogen bonds) and formamide (capable of two hydrogen bonds). These liquids have the highest surface tensions. Furthermore, the slopes of the linear approximations are about twice as much for all the hydrogen-bonded liquids. For instance, water has a slope of *ca.* -159 $\mu J.m^{-2}.K^{-1}$ whereas methylene iodide has a slope of *ca.* -80 $\mu J.m^{-2}.K^{-1}$. However, these observations on hydrogen bonds are not applicable for the general case. For instance, alcohols can have low surface tensions and comparatively weaker surface tension dependency on temperature.[13] Glycerol is an interesting liquid due to its high thermal stability, enabling contact angle measurements up to temperatures near 240°C.

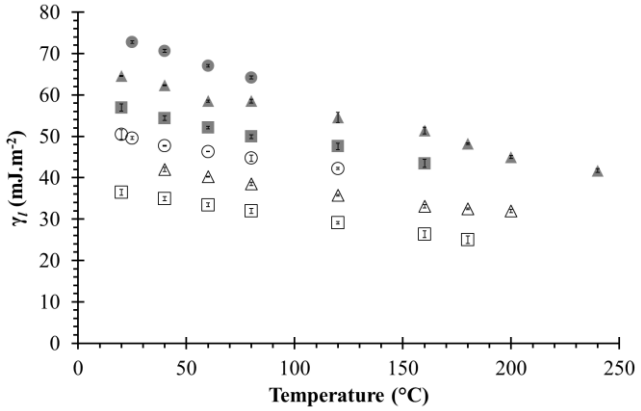

Figure 4. Surface tensions of water (●), glycerol (▲), formamide (■), methylene iodide (○), ethylene carbonate (△) and methyl benzoate (□) at various temperatures. Hydrogen-bonding liquids are represented with filled symbols.

4.3. Contact angles

4.3.1. Surface tension partitioning

In this part of the work, the goal was to determine the free surface energy of PTFE at various temperatures using equation (4) with the apolar liquid methylene iodide, following the models of Fowkes or Van Oss *et al.*[9,32,38,41] The results of the contact angles of methylene iodide as well as the calculated surface free energy of PTFE are given in Figure 5.

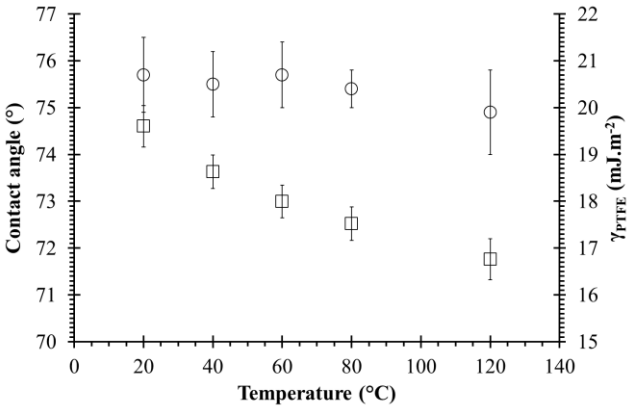

Figure 5. Contact angle of methylene iodide on PTFE (○) and surface free energy of PTFE (□) as a function of temperature. Error bars on γ_{PTFE} were calculated by propagation of uncertainty.

The variation of the contact angle of methylene iodide on PTFE is moderate. The calculated surface free energy of PTFE decreases with increasing temperatures, and this decrease is statistically significant when measurement errors are considered. The absolute γ_{PTFE} values are well in line with literature values.[31,70–72] However, Nardin and Schultz measured a γ_{PTFE} slope of -85 μJ.m^{-2}.K^{-1} whereas the slope determined here under the assumption of a linear decrease is -27 μJ.m^{-2}.K^{-1}.[70] Three things can explain this discrepancy. First of all, it was demonstrated by Neuman and Tanner that the surface free energy of PTFE varied non-linearly and this non-linearity could be attributed to the viscoelastic relaxations of the material.[28] Secondly, the surface free energy of PTFE is very sensitive to its molecular weight.[73] A molecular weight difference could account for deviations between the two results. Thirdly, there are experimental differences between the experimental protocol used here and that of Nardin and Schultz (liquids, surface preparation, polymer purity).

The surface free energy of PTFE was then used to calculate the dispersive components of the other liquids (Figure 6). Measured values were used for temperatures < 120°C and values extrapolated from the γ_{PTFE} slope were used for temperatures > 150°C. The extrapolation was that of the linear Eötvös approximation. Several facts emerge. Water at 25°C has a γ^{LW} component of about 23.00 ± 2.31 mJ.m^{-2}, a value consistent with the value of 21.8 ± 0.7 mJ.m^{-2} at 20°C reported by Fowkes using a two-liquid measurement method or by van Oss at 25°C using contact angle measurements.[32,41] In a similar way, the values reported for the other liquids such as glycerol, formamide or methylene iodide generally show excellent agreements with literature data (Table 2), demonstrating the validity and the robustness of the method at this temperature.

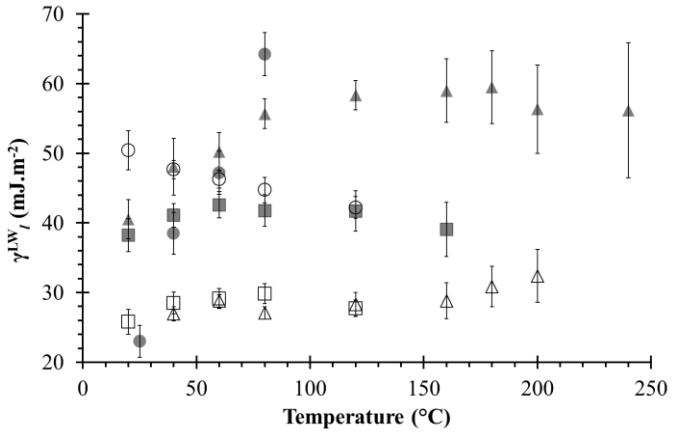

Figure 6. Calculated dispersive components of the surface tensions of water (●), glycerol (▲), formamide (■), methylene iodide (○), ethylene carbonate (△) and methyl benzoate (□) at various temperatures. All error bars were calculated by propagation of uncertainty.

Table 2. Surface tension partitioning of common liquids at room temperature (*: the variation of the uncertainty when compared to the experimental value is due to the backpropagation of the uncertainties in the calculation)

Liquid	γ_l (mJ.m^{-2})	γ_l^{LW} (mJ.m^{-2}) in this work	γ_l^{LW} (mJ.m^{-2}) ([32]) at 20°C	γ_l^{LW} (mJ.m^{-2}) ([41]) at 20°C
Water (25°C)	72.74 ± 0.34	23.00 ± 2.31	21.8 ± 0.7	21.8
Glycerol (20°C)	64.58 ±0.09	40.53 ± 2.83	37 ± 4	34.0
Methylene iodide (20°C)	50.42 ± 1.17	50.42 ± 2.82(*)	48.5 ± 9	50.8
Formamide (20°C)	56.93 ±0.88	38.22 ± 2.36	39.5 ± 7	39.0

However, the measurements showed an unexpected trend when the temperature was increased. For all the liquids except methylene iodide, γ^{LW} initially increased when the temperature was raised. The increase was monotonic in the case of water and ethylene carbonate. In the cases of glycerol, formamide, and methyl benzoate, a local maximum was reached before γ^{LW} decreased. Regarding water, γ^{LW} increased very much as soon as the temperature was increased and water appears as being fully dispersive at 80°C. This observation violates other measurements using a liquid-liquid method, for instance

using heptane drops in water, which show a slow decrease of γ^{LW}_{water} at a rate of ~ -24.5 $\mu J.m^{-2}.K^{-1}$.[74] Liquid-liquid methods are not prone to contact angle measurement artefacts and they are generally considered as more reliable. This low dependency of γ^{LW}_{water} was observed in other works.[41] One needs to further question the physical meaning of such a result by looking at vdW forces and hydrogen bonds in particular. vdW forces can slightly decrease as the temperature is increased due to a slight polarizability decrease. This is perfectly exemplified by methyl iodine here. By no means could these vdW forces increase when the temperature is raised. The polar bonds, such as hydrogen bonds, are known to be particularly sensitive to temperature and they are expected to decrease much faster than London forces, for instance. Therefore, the results that show an increase of γ^{LW} with the temperature are mere artifacts of the measuring conditions. Many other artifacts could be envisaged. For instance, one could expect the viscosity of glycerol to lead to long stabilization times before the static contact angle was reached; as its viscosity decreases rapidly with temperature, this contact angle bias could lessen at higher temperatures. Another corrective parameter, the spreading pressure, was always neglected in these calculations. Preliminary trials with this dataset have shown that the spreading pressure could vary non-linearly with some liquids. In the case of water, the calculated spreading pressure appeared as being negative, which is impossible, but could perhaps be explained by an undesired Cassie-Baxter state. In a similar way, the work of adhesion which should be linear and which should have a negative slope appeared non-linear for most liquids; it had a positive slope in the case of water.[40,75] The alternative use of the equation of state was unfruitful too.[76,77] Eventually, even small polar interactions between PTFE and the liquids were not sufficient to explain the observed deviations. These results therefore reinforced the conclusions that are already found in the literature about the static contact angle: the contact angle can hardly be predicted by the so-called partitioning models because they are not thermodynamically valid.[40,75,78,79]Hence, an alternative model was built to give an explanation of the measured contact angles as a function of temperature, and this interpretation needed to depart from the most classical partitioning theories. A different view is thus proposed in the next subsection.

4.3.2. Alternative model: a transition state approach

Contact angle measurements should be considered pragmatically because they convolute many factors. For instance, the liquid has a given purity. In parallel, surface impurities or solid compositional variations are known to greatly affect droplet spreading and wetting. Real-life solids will affect liquid spreading by convoluting the effects of chemical surface heterogeneities, surface roughness and surface impurities with the spread of the droplet. Equation (16) is an attempt to describe a droplet macroscopic contact angle without any *a priori* knowledge of each one of these effects. However, all of these effects could be thought as entering the potential energy terms and equation (16) could constitute a universal approach. Plots were therefore drawn to test the linearity of the relationship between predicted and measured samples by adjusting the cutoff length $< d >$ and the fractal dimension f (Figure 7). In some cases, only two or less measurements (temperatures) could be performed before total wetting occurred; these results were discarded from the graphs but the two temperature points are presented in Table 3 (*).

Looking at the results provided by the fitting, the model seems in conformity with the basic assumptions: the fractal dimension f is usually found to be below 3, as expected. The cutoff length $< d >$ is usually in the order of an interatomic distance. The fits are also very good and the linear regression is successful, with an average coefficient of determination of 96%. We found $f = 3$ for water on PTFE, which is somewhat consistent with the hypothesis of a Cassie-Baxter state, as explained in 2.2. Some more results set the PTFE apart from the other materials. In particular, the values of $< d >$ are the highest ones among all solids for each liquid. Once again, this is expected as PTFE is the only macromolecular material tested here: if $< d >$ can be thought as the correlation distance between adsorption sites (or finite potential wells), then it makes sense to find the highest values for PTFE.

Another value stands apart from the rest: the f value of water on stainless steel is 3.25. However, the model used so far is true for a monomodal potential distribution, *i.e.* one with a unique $< d >$. If one wants to set equation (14) in a more general framework, then the partition function ratio would become:

$$\frac{F^{\ddagger}_{ads}}{F^{\ddagger}_{des}} = \prod_{i \in \mathbb{N}} \left(\frac{\xi}{\langle d_i \rangle} \right)^{f_i} \qquad (17)$$

Equation (17) allows ξ to bear an exponent > 3. Composite surfaces could behave that way, and the grain boundaries found in stainless steel might "probe" water molecules differently from the inner grain surface.

Methyl benzoate has consistently low f values across the whole dataset, it completely wets zirconia and it is the liquid that has the lowest contact angles on PTFE (Figure 3). Since this liquid is the only one tested here bearing an aromatic cycle capable of π-interactions, this peculiar behavior might be explained by its aromatic ring, and therefore to its specific chemistry.

Eventually, the sensitivity of the model was tested with a dataset in which noise was introduced in the contact angle and surface tension values. The example of glycerol on steel was chosen because of its size. This dataset was also well described by the model initially: the correlation was good (Table 3) and the deviation between the model and the experiment was rather stable across the whole temperature range. At first, an ideal contact angle dataset was calculated based on the basis of the $<d>$ and f parameters determined in this work and also on the basis of the glycerol surface tension data provided by Petke (1969), because it fitted

closely our experimental results.[23] Then, approximate simulated values were generated randomly on the basis of a normal distribution centered around the ideal values (= average θ or γ) and standard deviations σ were introduced. We chose σ_θ = 0.5, 1, 2 and 3° and σ_γ = 0.1, 0.5, 1, and 2 $mJ.m^{-2}$. Three situations were studied: noise was introduced to the contact angle, to the surface tension and to both variables (combined randomization effect). Then, the average deviation across the whole temperature range (9 values between 20 and 240°C) and between predicted and ideal contact angles were calculated on the basis of 100 runs (100 noisy datasets were generated). The results show the relative sensitivity of the model (Figure 8).

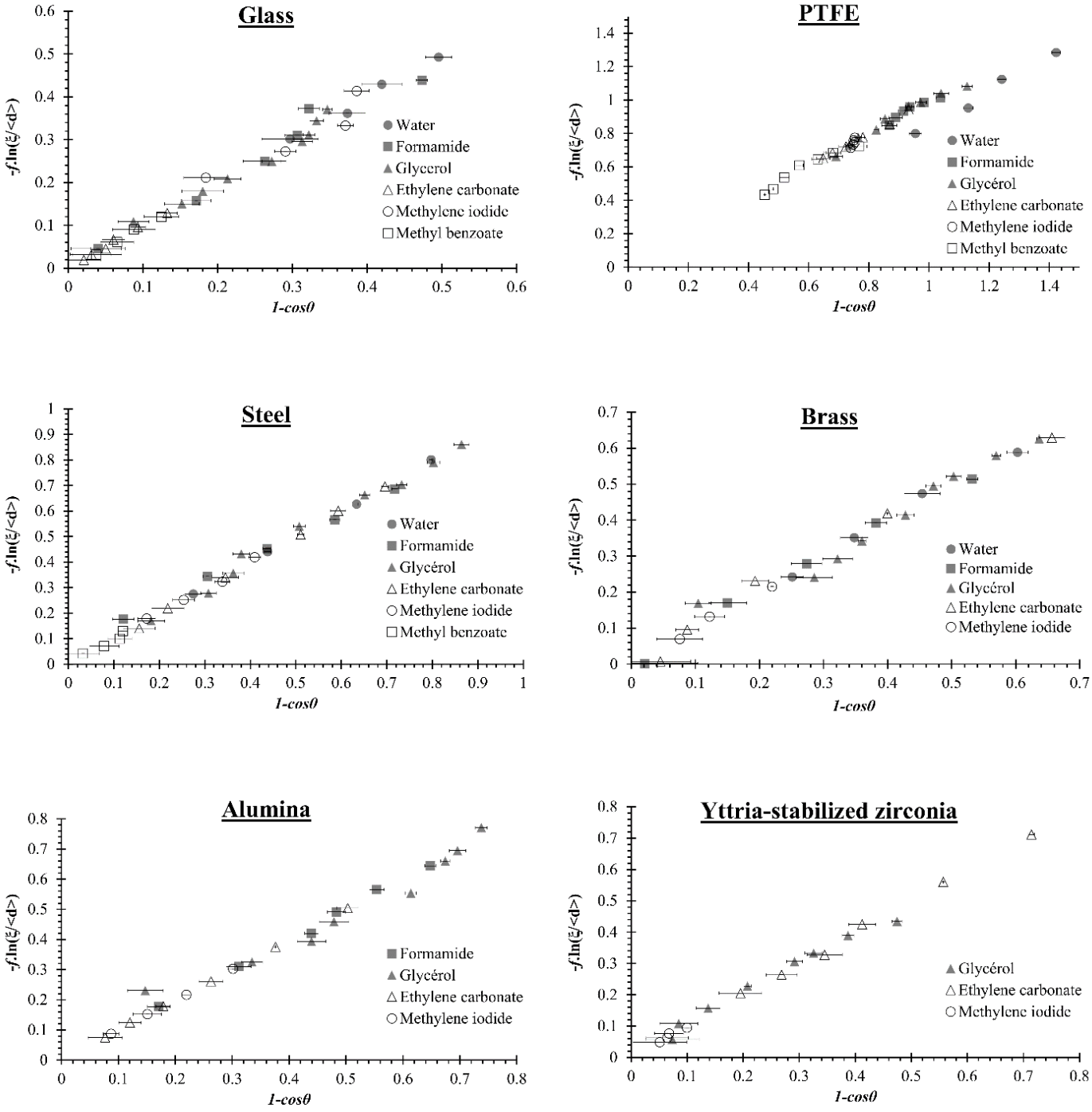

Figure 7. Plots of the results obtained by describing the static contact angle using the proposed model for a set of six solid surfaces and using six liquids with temperatures varying from 20 to 240°C.

Table 3. Table showing the fractal dimension f, the cutoff length $< d >$ and the coefficient of determination obtained for all liquids on all substrates and at all temperatures. In some cases, total wetting prevented to perform the contact angle measurements (denoted as "n.a." in the table). Other fits (*) were performed on only two points when only two temperatures were available in order to produce f and $< d >$ values for discussion.

Substrate	Model parameters	Water	Formamide	Glycerol	Ethylene carbonate	Methylene iodide	Methyl benzoate
Glass	f	1.18	1.19	0.53	0.32	1.32	0.56
	$< d >$ (Å)	3.56	3.86	5.07	4.80	3.87	4.14
	R^2	0.9870	0.9619	0.9683	0.9902	0.8724	0.9863
PTFE	f	3.00	0.50	0.84	0.85	0.26	0.71
	$< d >$ (Å)	3.60	20.09	9.06	9.73	56.03	9.19
	R^2	0.9886	0.9069	0.9695	0.9941	0.7488	0.9375
Stainless steel	f	3.25	2.16	1.38	1.83	1.57	0.56
	$< d >$ (Å)	3.00	3.67	4.66	4.69	3.70	4.21
	R^2	0.9996	0.9716	0.9871	0.9983	0.9880	0.9076
Brass	f	2.14	2.16	0.92	2.05	1.36	0.19
	$< d >$ (Å)	3.09	3.38	4.96	4.36	3.32	4.33
	R^2	0.9898	0.9920	0.9584	0.9841	0.9862	1 (*)
Alumina	f	n.a.	1.41	1.20	1.25	1.41	0.09
	$< d >$ (Å)	n.a.	4.21	4.99	4.80	3.51	4.96
	R^2	n.a.	0.9957	0.9561	0.9998	0.9995	1(*)
Zirconia	f	n.a.	n.a.	0.90	1.48	0.30	n.a.
	$< d >$ (Å)	n.a.	n.a.	4.06	5.20	3.88	n.a.
	R^2	n.a.	n.a.	0.9774	0.9967	0.9139	n.a.

In Figure 8, the horizontal dotted line corresponds to the average deviation between our experimental values (physically measured) and the ideal case. Since average contact angles are given with a standard deviation better than 2° and surface tensions are given with a standard deviation better than 1 $mJ.m^{-2}$ (see raw data), then a conservative estimate would be that of the third case in the combined randomization case (dark grey bars, σ_θ = 2° and σ_γ = 1 $mJ.m^{-2}$). The deviation between the predicted and the true contact angles wouldn't exceed 1.7° ± 0.4°. Another test was performed using random noise fluctuations around the average values (equal probabilities were assumed between lower and upper bounds centered around the mean value, in contrast with the normal distribution that has no cutoff), and the method appeared to predict theta with a deviation better than 1° for measurement errors with θ fluctuations of 2° around their average and γ fluctuations of 1 mJ/m^2 around their average. As a consequence, the model appears to predict meaningful contact angles with experimentally realistic noise levels.

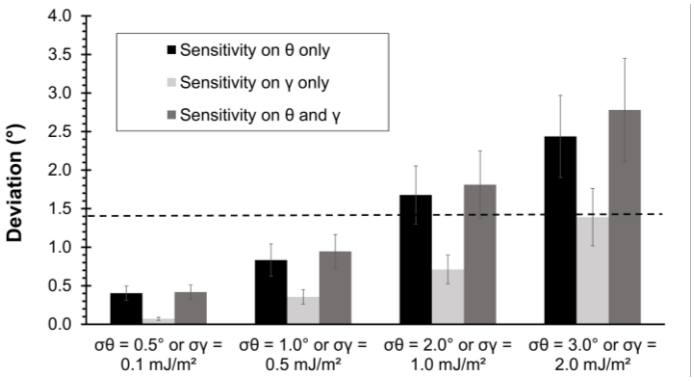

Figure 8. Deviation of the contact angle between simulated values and the "ideal" predicted values. The simulated values were distributed according to a normal distribution with standard deviations σ_θ and σ_γ. The simulation was performed in the case of glycerol on steel (f = 1.38 and $<d>$ = 4.66 Å). The dotted line shows the deviation between our experiment and the ideal case.

5. Conclusions

In this work, the thermal variations of contact angles were studied for a wide range of liquids and solids. Two theories were tested in order to find a general predictive model. A novel transition state model succeeded where the surface tension partitioning was useful only for room temperature results.

In the first approach, surface tension partitioning was applied. Two main concerns emerged.[40,75,79] The first concern is that the surface tension partitioning theory is an oversimplification of the surface enthalpy partitioning

theory. Whereas the energetic (or enthalpic) part of the surface tension should be ruled by intermolecular interactions, there is no reason why the entropic part of it should obey the same rule. In other words, the use of surface tension partitioning "works" at a given temperature because of its self-consistency; it could however fail when the temperature is varied. This was observed in the present work: surface tension partitioning was well in line with literature data near room temperature, but it failed at being useful when the temperature was increased (Figure 6).[32,41] The other concern is related to the use of the molecular interaction partitioning with contact angle measurements: the importance of the *microscopic* parameters (molecular interactions) could be small before the other parameters (such as triple line pinning) that dictate the value of the measured *macroscopic* contact angle.[75] As a consequence, one feels the subtle significance of the temperature parameter for any wetting measurement using the contact angle method.

A second model was therefore built. This model is based on the transition state theory and could be seen as a static treatment of the molecular kinetic theory used for dynamic contact angles.[34,36,37] This model encompasses regular wetting but also wetting on real surfaces, *i.e.* Cassie-Baxter or Wenzel states, and the transition to complete wetting. A causal hypothesis is put forward: the triple line distortion subrogates the thermocapillary vibration at the interface and the liquid molecules near the triple line are adsorbed against a set of spatially correlated adsorption sites. By combining this hypothesis with the equation of state, a very good description (Figure 7 and Table 3) of the static contact angle variations with temperature could be provided for a large set of materials representing real surfaces, using only two comprehensible variables, a fractal dimension f and a cutoff length $< d >$. This theory seems valid for a very wide range of contact angles, including contact angles > 90°. Therefore, it proved superior to surface tension partitioning as long as thermal effects were the main purpose of study. This result is also congruent with the view of Prevost *et al.* which stated that the triple line advances through thermally-activated jumps.[80]

This theory does not at present cover the case of macromolecular liquids, polymer solutions or suspensions, which will be the topic of further investigations. The use of surfaces with tailored surface roughness will be further studied. In the future, the model will be tested with different bulk vapors and using the two liquid phases method; the latter can be used to tailor surface wave amplitude.[43,81]

Declaration of Competing Interest

The authors declare that they have no known competing financial interests or personal relationships that could have appeared to influence the work reported in this paper.

CRediT author statement

Joël Bréard: Supervision, Reviewing. **Guillaume Cazaux:** Investigation, Reviewing. **Benoît Duchemin:** Formal analysis, Writing- Original draft preparation, Supervision. **Moussa Gomina:** Supervision, Project administration.

Acknowledgement

The contact angles used in this work were acquired as part of the TAPAS project and it was funded by the French National Research Agency (grant number ANR-11-RMNP-0020). The authors are indebted to Michel Nardin (INC, CNRS) for his kind advises.

Please cite as:

Duchemin, B., Cazaux, G., Gomina, M., Bréard, J., 2021. Temperature-dependence of the static contact angle: A transition state theory approach. Journal of Colloid and Interface Science 592, 215–226. https://doi.org/10.1016/j.jcis.2021.02.059

References

(1) Quéré, D. Wetting and Roughness. *Annu. Rev. Mater. Res.* **2008**, *38* (1), 71–99. https://doi.org/10.1146/annurev.matsci.38.060407.132434.

(2) Wang, G.; He, Y.; Wang, H.; Zhang, L.; Yu, Q.; Peng, S.; Wu, X.; Ren, T.; Zeng, Z.; Xue, Q. A Cellulose Sponge with Robust Superhydrophilicity and Under-Water Superoleophobicity for Highly Effective Oil/Water Separation. *Green Chem.* **2015**, *17* (5), 3093–3099. https://doi.org/10.1039/C5GC00025D.

(3) Nishino, T.; Meguro, M.; Nakamae, K.; Matsushita, M.; Ueda, Y. The Lowest Surface Free Energy Based on –CF3 Alignment. *Langmuir* **1999**, *15* (13), 4321–4323. https://doi.org/10.1021/la981727s.

(4) Li, X.-M.; Reinhoudt, D.; Crego-Calama, M. What Do We Need for a Superhydrophobic Surface? A Review on the Recent Progress in the Preparation of Superhydrophobic Surfaces. *Chem. Soc. Rev.* **2007**, *36* (8), 1350–1368.

(5) Eötvös, R. Ueber Den Zusammenhang Der Oberflächenspannung Der Flüssigkeiten Mit Ihrem Molecularvolumen. *Ann. Phys.* **1886**, *263* (3), 448–459. https://doi.org/10.1002/andp.18862630309.

(6) Macleod, D. B. On a Relation between Surface Tension and Density. *Trans Faraday Soc* **1923**, *19* (July), 38–41.

(7) De Gennes, P.-G.; Brochard-Wyart, F.; Quéré, D. *Capillarity and Wetting Phenomena: Drops, Bubbles, Pearls, Waves*; Springer, 2004.

(8) Ono, S.; Kondo, S. Molecular Theory of Surface Tension in Liquids. In *Structure of Liquids / Struktur der Flüssigkeiten*; Encyclopedia of Physics

/ Handbuch der Physik; Springer Berlin Heidelberg, 1960; pp 134–280. https://doi.org/10.1007/978-3-642-45947-4_2.
(9) Van Oss, C. J. *Interfacial Forces in Aqueous Media*; CRC press, 2006.
(10) Kayser, W. V. Temperature Dependence of the Surface Tension of Water in Contact with Its Saturated Vapor. *J. Colloid Interface Sci.* **1976**, *56* (3), 622–627. https://doi.org/10.1016/0021-9797(76)90130-2.
(11) Ramsay, W.; Shields, J. The Variation of Molecular Surface-Energy with Temperature. *Philos. Trans. R. Soc. Math. Phys. Eng. Sci.* **1893**, *184* (0), 647–673. https://doi.org/10.1098/rsta.1893.0013.
(12) Palit, S. R. Thermodynamic Interpretation of the Eötvös Constant. *Nature* **1956**, *177* (4521), 1180–1180. https://doi.org/10.1038/1771180a0.
(13) Pászli, I.; László, K. Molar Surface Energy and Eötvös's Law. *Colloid Polym. Sci.* **2007**, *285* (13), 1505–1508. https://doi.org/10.1007/s00396-007-1723-8.
(14) Lennard-Jones, J. E.; Corner, J. The Calculation of Surface Tension from Intermolecular Forces. *Trans. Faraday Soc.* **1940**, *36*, 1156–1162.
(15) Perez-Diaz, J. L.; Alvarez-Valenzuela, M. A.; Sanchez-Garcia-Casarrubios, J.; Jimenez-Lopez, S. Ice Surface Entropy Induction by Humidity or How Humidity Prompts Freezing. *J. Multidiscip. Eng. Sci. Technol.* **2016**, *3* (1), 3825–3828.
(16) Ferguson, A. On a Relation between Surface Tension and Density. *Trans. Faraday Soc.* **1923**, *19* (November), 407–412.
(17) Guggenheim, E. A. The Principle of Corresponding States. *J. Chem. Phys.* **1945**, *13* (7), 253–261. https://doi.org/10.1063/1.1724033.
(18) Dee, G. T.; Sauer, B. B. The Molecular Weight and Temperature Dependence of Polymer Surface Tension: Comparison of Experiment with Interface Gradient Theory. *J. Colloid Interface Sci.* **1992**, *152* (1), 85–103. https://doi.org/10.1016/0021-9797(92)90010-J.
(19) Sauer, B. B.; Dee, G. T. Surface Tension and Melt Cohesive Energy Density of Polymer Melts Including High Melting and High Glass Transition Polymers. *Macromolecules* **2002**, *35* (18), 7024–7030. https://doi.org/10.1021/ma0202437.
(20) Dee, G. T.; Ougizawa, T.; Walsh, D. J. The Pressure-Volume-Temperature Properties of Polyethylene, Poly(Dimethyl Siloxane), Poly(Ethylene Glycol) and Poly(Propylene Glycol) as a Function of Molecular Weight. *Polymer* **1992**, *33* (16), 3462–3469. https://doi.org/10.1016/0032-3861(92)91104-A.
(21) Berim, G. O.; Ruckenstein, E. Dependence of the Macroscopic Contact Angle on the Liquid-Solid Interaction Parameters and Temperature. *J. Chem. Phys.* **2009**, *130* (18), 184712. https://doi.org/10.1063/1.3133327.
(22) de Ruijter, M.; Kölsch, P.; Voué, M.; De Coninck, J.; Rabe, J. P. Effect of Temperature on the Dynamic Contact Angle. *Colloids Surf. Physicochem. Eng. Asp.* **1998**, *144* (1–3), 235–243. https://doi.org/10.1016/S0927-7757(98)00659-1.
(23) Petke, F. D.; Ray, B. R. Papers Presented at the 43rd National Colloid SymposiumTemperature Dependence of Contact Angles of Liquids on Polymeric Solids. *J. Colloid Interface Sci.* **1969**, *31* (2), 216–227. https://doi.org/10.1016/0021-9797(69)90329-4.
(24) Gribanova, E. V. Dynamic Contact Angles: Temperature Dependence and the Influence of the State of the Adsorption Film. *Adv. Colloid Interface Sci.* **1992**, *39*, 235–255. https://doi.org/10.1016/0001-8686(92)80062-3.
(25) Zisman, W. A. Relation of the Equilibrium Contact Angle to Liquid and Solid Constitution. In *Contact Angle, Wettability and Adhesion*; Advances in Chemistry; American Chemical Society: Washington DC, 1964; pp 1–51.
(26) Bernardin, J. D.; Mudawar, I.; Walsh, C. B.; Franses, E. I. Contact Angle Temperature Dependence for Water Droplets on Practical Aluminum Surfaces. *Int. J. Heat Mass Transf.* **1997**, *40* (5), 1017–1033. https://doi.org/10.1016/0017-9310(96)00184-6.
(27) Adamson, A. W. Potential Distortion Model for Contact Angle and Spreading. II. Temperature Dependent Effects. *J. Colloid Interface Sci.* **1973**, *44* (2), 273–281. https://doi.org/10.1016/0021-9797(73)90219-1.
(28) Neumann, A. W.; Tanner, W. The Temperature Dependence of Contact Angles—Polytetrafluoroethylene/n-Decane. *J. Colloid Interface Sci.* **1970**, *34* (1), 1–8. https://doi.org/10.1016/0021-9797(70)90252-3.
(29) Della Volpe, C.; Maniglio, D.; Brugnara, M.; Siboni, S.; Morra, M. The Solid Surface Free Energy Calculation: I. In Defense of the Multicomponent Approach. *J. Colloid Interface Sci.* **2004**, *271* (2), 434–453. https://doi.org/10.1016/j.jcis.2003.09.049.
(30) Jańczuk, B.; Białopiotrowicz, T.; Wójcik, W. The Components of Surface Tension of Liquids and Their Usefulness in Determinations of Surface Free Energy of Solids. *J. Colloid Interface Sci.* **1989**, *127* (1), 59–66. https://doi.org/10.1016/0021-9797(89)90007-6.
(31) Owens, D. K.; Wendt, R. C. Estimation of the Surface Free Energy of Polymers. *J. Appl. Polym. Sci.* **1969**, *13* (8), 1741–1747. https://doi.org/10.1002/app.1969.070130815.
(32) Fowkes, F. M. Attractive Forces at Interfaces. *Ind. Eng. Chem.* **1964**, *56* (12), 40–52. https://doi.org/10.1021/ie50660a008.

(33) Brochard-Wyart, F.; De Gennes, P. G. Dynamics of Partial Wetting. *Adv. Colloid Interface Sci.* **1992**, *39*, 1–11.
(34) Blake, T. D.; Haynes, J. M. Kinetics of Liquid/Liquid Displacement. *J. Colloid Interface Sci.* **1969**, *30* (3), 421–423. https://doi.org/10.1016/0021-9797(69)90411-1.
(35) Eyring, H. The Theory of Absolute Reaction Rates. *Trans. Faraday Soc.* **1938**, *34* (0), 41–48. https://doi.org/10.1039/TF9383400041.
(36) Pucci, M. F.; Duchemin, B.; Gomina, M.; Bréard, J. Dynamic Wetting of Molten Polymers on Cellulosic Substrates: Model Prediction for Total and Partial Wetting. *Front. Mater.* **2020**, *7*. https://doi.org/10.3389/fmats.2020.00143.
(37) Blake, T. D. The Physics of Moving Wetting Lines. *J. Colloid Interface Sci.* **2006**, *299* (1), 1–13.
(38) Van Oss, C. J.; Good, R. J.; Chaudhury, M. K. Additive and Nonadditive Surface Tension Components and the Interpretation of Contact Angles. *Langmuir* **1988**, *4* (4), 884–891. https://doi.org/10.1021/la00082a018.
(39) Żenkiewicz, M. Methods for the Calculation of Surface Free Energy of Solids. *J. Achiev. Mater. Manuf. Eng.* **2007**, *24* (1), 137–145.
(40) Lyklema, J. The Surface Tension of Pure Liquids: Thermodynamic Components and Corresponding States. *Colloids Surf. Physicochem. Eng. Asp.* **1999**, *156* (1–3), 413–421. https://doi.org/10.1016/S0927-7757(99)00100-4.
(41) van Oss, C. J. Acid—Base Interfacial Interactions in Aqueous Media. *Colloids Surf. Physicochem. Eng. Asp.* **1993**, *78*, 1–49. https://doi.org/10.1016/0927-7757(93)80308-2.
(42) Joud, J.-C.; Barthes-Labrousse, M.-G. *Physico-chimie des surfaces et acido-basicité*; ISTE Editions, 2015.
(43) Aarts, D. G. A. L.; Schmidt, M.; Lekkerkerker, H. N. W. Direct Visual Observation of Thermal Capillary Waves. *Science* **2004**, *304* (5672), 847–850. https://doi.org/10.1126/science.1097116.
(44) Sanyal, M. K.; Sinha, S. K.; Huang, K. G.; Ocko, B. M. X-Ray-Scattering Study of Capillary-Wave Fluctuations at a Liquid Surface. *Phys. Rev. Lett.* **1991**, *66* (5), 628–631. https://doi.org/10.1103/PhysRevLett.66.628.
(45) Ocko, B. M.; Wu, X. Z.; Sirota, E. B.; Sinha, S. K.; Deutsch, M. X-Ray Reflectivity Study of Thermal Capillary Waves on Liquid Surfaces. *Phys. Rev. Lett.* **1994**, *72* (2), 242–245. https://doi.org/10.1103/PhysRevLett.72.242.
(46) Derks, D.; Aarts, D. G. A. L.; Bonn, D.; Lekkerkerker, H. N. W.; Imhof, A. Suppression of Thermally Excited Capillary Waves by Shear Flow. *Phys. Rev. Lett.* **2006**, *97* (3), 038301. https://doi.org/10.1103/PhysRevLett.97.038301.
(47) Schwartz, D. K.; Schlossman, M. L.; Kawamoto, E. H.; Kellogg, G. J.; Pershan, P. S.; Ocko, B. M. Thermal Diffuse X-Ray-Scattering Studies of the Water-Vapor Interface. *Phys. Rev. A* **1990**, *41* (10), 5687–5690. https://doi.org/10.1103/PhysRevA.41.5687.
(48) Belardinelli, D.; Sbragaglia, M.; Gross, M.; Andreotti, B. Thermal Fluctuations of an Interface near a Contact Line. *Phys. Rev. E* **2016**, *94* (5), 052803. https://doi.org/10.1103/PhysRevE.94.052803.
(49) Leger, L.; Joanny, J. F. Liquid Spreading. *Rep. Prog. Phys.* **1992**, *55* (4), 431. https://doi.org/10.1088/0034-4885/55/4/001.
(50) Delmas, M.; Monthioux, M.; Ondarçuhu, T. Contact Angle Hysteresis at the Nanometer Scale. *Phys. Rev. Lett.* **2011**, *106* (13), 136102.
(51) Robbins, M. O.; Joanny, J. F. Contact Angle Hysteresis on Random Surfaces. *EPL Europhys. Lett.* **1987**, *3* (6), 729. https://doi.org/10.1209/0295-5075/3/6/013.
(52) Eyring, H. The Activated Complex and the Absolute Rate of Chemical Reactions. *Chem. Rev.* **1935**, *17* (1), 65–77.
(53) Laidler, K. J.; King, M. C. The Development of Transition-State Theory. *J. Phys. Chem.* **1983**, *87* (15), 2657–2664.
(54) Eyring, H. The Activated Complex in Chemical Reactions. *J. Chem. Phys.* **1935**, *3* (2), 107–115.
(55) Léger, L.; Hervet, H.; Massey, G.; Durliat, E. Wall Slip in Polymer Melts. *J. Phys. Condens. Matter* **1997**, *9* (37), 7719–7740. https://doi.org/10.1088/0953-8984/9/37/006.
(56) Indekeu, J. O. How Universal Is Critical-Point Wetting? *Phys. Stat. Mech. Its Appl.* **1991**, *177* (1), 428–436. https://doi.org/10.1016/0378-4371(91)90183-D.
(57) Bonn, D.; Eggers, J.; Indekeu, J.; Meunier, J.; Rolley, E. Wetting and Spreading. *Rev. Mod. Phys.* **2009**, *81* (2), 739–805. https://doi.org/10.1103/RevModPhys.81.739.
(58) de Gennes, P. G. Wetting: Statics and Dynamics. *Rev. Mod. Phys.* **1985**, *57* (3), 827–863. https://doi.org/10.1103/RevModPhys.57.827.
(59) Shafrin, E. G.; Zisman, W. A. Effect of Temperature on Wetting of High- and Low-Energy Solid Surfaces. *J. Phys. Chem.* **1972**, *76* (22), 3259–3267. https://doi.org/10.1021/j100666a025.
(60) Ragil, K.; Meunier, J.; Broseta, D.; Indekeu, J. O.; Bonn, D. Experimental Observation of Critical Wetting. *Phys. Rev. Lett.* **1996**, *77* (8), 1532–1535. https://doi.org/10.1103/PhysRevLett.77.1532.
(61) Bonn, D.; Ross, D. Wetting Transitions. *Rep. Prog. Phys.* **2001**, *64* (9), 1085. https://doi.org/10.1088/0034-4885/64/9/202.
(62) Song, B.; Springer, J. Determination of Interfacial Tension from the Profile of a Pendant Drop Using

Computer-Aided Image Processing: 1. Theoretical. *J. Colloid Interface Sci.* **1996**, *184* (1), 64–76. https://doi.org/10.1006/jcis.1996.0597.
(63) Song, B.; Springer, J. Determination of Interfacial Tension from the Profile of a Pendant Drop Using Computer-Aided Image Processing: 2. Experimental. *J. Colloid Interface Sci.* **1996**, *184* (1), 77–91. https://doi.org/10.1006/jcis.1996.0598.
(64) Haynes, W. M. *CRC Handbook of Chemistry and Physics, 95th Edition*; CRC Press, 2014.
(65) Grigoriev, I. S.; Meilikhov, E. Z.; Radzig, A. A. Handbook of Physical Quantities (November 25, 1996 Ed.). *TF-CRC* **1997**, *32*, 92.
(66) Rathnam, M. V.; Mankumare, S.; Kumar, M. S. S. Density, Viscosity, and Speed of Sound of (Methyl Benzoate + Cyclohexane), (Methyl Benzoate + n-Hexane), (Methyl Benzoate + Heptane), and (Methyl Benzoate + Octane) at Temperatures of (303.15, 308.15, and 313.15) K. *J. Chem. Eng. Data* **2010**, *55* (3), 1354–1358. https://doi.org/10.1021/je9006597.
(67) Zheng, Q.-S.; Yu, Y.; Zhao, Z.-H. Effects of Hydraulic Pressure on the Stability and Transition of Wetting Modes of Superhydrophobic Surfaces. *Langmuir* **2005**, *21* (26), 12207–12212. https://doi.org/10.1021/la052054y.
(68) Gharagheizi, F.; Eslamimanesh, A.; Tirandazi, B.; Mohammadi, A. H.; Richon, D. Handling a Very Large Data Set for Determination of Surface Tension of Chemical Compounds Using Quantitative Structure–Property Relationship Strategy. *Chem. Eng. Sci.* **2011**, *66* (21), 4991–5023. https://doi.org/10.1016/j.ces.2011.06.052.
(69) Sheu, Y.-W.; Tu, C.-H. Densities, Viscosities, Refractive Indices, and Surface Tensions for 12 Flavor Esters from T = 288.15 K to T = 358.15 K. *J. Chem. Eng. Data* **2005**, *50* (5), 1706–1710. https://doi.org/10.1021/je050170x.
(70) Nardin, M.; Schultz, J. Considérations sur l'adsorption de n-alcanes et de perfluoroalcanes à la surface de polymères de même structure chimique. *J. Chim. Phys.* **1990**, *87* (4), 539–554.
(71) Grundke, K.; Augsburg, A. On the Determination of the Surface Energetics of Porous Polymer Materials. *J. Adhes. Sci. Technol.* **2000**, *14* (5), 765–775. https://doi.org/10.1163/156856100742861.
(72) Van Oss, C. J.; Good, R. J.; Chaudhury, M. K. The Role of van Der Waals Forces and Hydrogen Bonds in "Hydrophobic Interactions" between Biopolymers and Low Energy Surfaces. *J. Colloid Interface Sci.* **1986**, *111* (2), 378–390. https://doi.org/10.1016/0021-9797(86)90041-X.
(73) Dettre, R. H.; Johnson, R. E. Concerning the Surface Tension, Critical Surface Tension, and Temperature Coefficient of Surface Tension of Poly(Tetrafluoroethylene). *J. Phys. Chem.* **1967**, *71* (5), 1529–1531. https://doi.org/10.1021/j100864a056.
(74) Peixinho, J.; Ageorges, V.; Duchemin, B. Growth of Clathrate Hydrates from Water Drops in Cyclopentane. *Energy Fuels* **2018**, *32* (3), 2693–2698. https://doi.org/10.1021/acs.energyfuels.7b02740.
(75) Weber, C.; Stanjek, H. Energetic and Entropic Contributions to the Work of Adhesion in Two-Component, Three-Phase Solid–Liquid–Vapour Systems. *Colloids Surf. Physicochem. Eng. Asp.* **2014**, *441*, 331–339. https://doi.org/10.1016/j.colsurfa.2013.07.034.
(76) Neumann, A. W. Contact Angles and Their Temperature Dependence: Thermodynamic Status, Measurement, Interpretation and Application. *Adv. Colloid Interface Sci.* **1974**, *4* (2), 105–191. https://doi.org/10.1016/0001-8686(74)85001-3.
(77) Neumann, A. W.; Good, R. J.; Hope, C. J.; Sejpal, M. An Equation-of-State Approach to Determine Surface Tensions of Low-Energy Solids from Contact Angles. *J. Colloid Interface Sci.* **1974**, *49* (2), 291–304. https://doi.org/10.1016/0021-9797(74)90365-8.
(78) Ghasemi, H.; Ward, C. A. Sessile-Water-Droplet Contact Angle Dependence on Adsorption at the Solid–Liquid Interface. *J. Phys. Chem. C* **2010**, *114* (11), 5088–5100. https://doi.org/10.1021/jp911259n.
(79) Douillard, J. M. Concerning the Thermodynamic Consistency of the "Surface Tension Components" Equations. *J. Colloid Interface Sci.* **1997**, *188* (2), 511–515. https://doi.org/10.1006/jcis.1997.4768.
(80) Prevost, A.; Rolley, E.; Guthmann, C. Thermally Activated Motion of the Contact Line of a Liquid ${}^{4}\mathrm{He}$ Meniscus on a Cesium Substrate. *Phys. Rev. Lett.* **1999**, *83* (2), 348–351. https://doi.org/10.1103/PhysRevLett.83.348.
(81) Schultz, J.; Nardin, M. Determination of the Surface Energy of Solids by the Two-Liquid-Phase Method. In *Modern Approaches to Wettability*; Schrader, M. E., Loeb, G. I., Eds.; Springer US, 1992; pp 73–100. https://doi.org/10.1007/978-1-4899-1176-6_4.